Aluminum Doping Contents Dependent Photoluminescence and Resistivity of ZnO Nanofilms

Aluminum Doping Contents Dependent Photoluminescence and Resistivity of ZnO Nanofilms

H.J.Al-Asedy[1],S.A. Al-khafaji[2], A. A. Salim[3]and H. Bakhtiar[3]

[1] Physics Department, Faculty of Education, University of Al-Qadisiyah, Diwaniyah 00964, Iraq
[2] Roads and Transports Department, Faculty of Engineering, University of Al-Qadisiyah, Diwaniyah 00964, Iraq
[3]Laser Center and Physics Department, Faculty of Science, UniversitiTeknologi Malaysia, 81310 Johor Bahru, Johor, Malaysia

Email: asali@utm.my

Abstract: Using sol–gel spin-coating technique Al-doped ZnO nanofilms (AZONFs) were made on Si(100) substrates and characterized. The obtained nanofilms were annealed at 500 ºC for 3 h in air. The effects of changing Al doping level (0 to 5 at%) on the structures, morphologies, electrical and photoluminescence characteristics of the nanofilms were evaluated. The XRD patterns of the AZONFs confirmed the formation of wurtzite hexagonal ZnO lattice with preferred growth along (101) lattice plane. In addition, the c-axis orientation of the AZONFs became weaker with the increase in Al doping contents. The surface morphologies, structures, electrical and optical properties of the AZONFs were found to be very sensitive to the Al contents changes. The nanofilm prepared with 1 at% of Al displayed lowest resistivity of 4.238×10^{-3} Ω.cm measured by the four-point probe method. The optical band gap energy (increased from 3.22 to 3.304 eV) and carrier mobility of the AZONFs were improved with the increase in Al contents. The proposed AZONFs may be advantageous for various high performance optoelectronic device applications.

1. Introduction

The wide band gap (3.37 eV) semiconductor Zinc Oxide (ZnO) is a technologically versatile material due to its interesting optical and electrical traits including the resistivity in the range of 10^{-3}–10^{5} Ω.cm, strong photoluminescence [1] and large exciton binding energy (60 meV) [2]. Certainly, being a transparent semiconducting oxide material ZnO thin films (ZOTFs) became prospective for various optoelectronic and biomedical applications [3]. Several studies showed that the high resistivity of the stoichiometric ZOTFs can be lowered either by incorporating oxygen vacancy (act as donor) or using dopants from group III (e.g. Al, Ga or In) [4]. The excellent optical transmittance in the visible range of the solar spectra and electrical conductivity of ZOTFs make it very useful for photovoltaic applications [5]. Recent study revealed that the

resistivity of ZOTFs can remarkably be lowered via Al doping which is also preferred because of easy inclusion in the ZnO crystal lattice without damaging its optical transmittance of the material [6]. In addition, the material Al and ZnO both are nontoxic, inexpensive and plentiful for the production of low resistive Al-doped ZOTFs with high optical transmittance in visible and near infrared (NIR) spectral region [7].

The Al contents dependent changes in the structural, optical and electrical characteristics of ZOTFs has been investigated [8]. Additionally, different synthesis methods have been used to grow ZOTFs including the pulse laser deposition (PLD) [9], chemical vapour deposition (CVD) [10] , radio frequency magnetron sputtering (RFMS) [11], electro-deposition (ED) [12] , spray pyrolysis (SP) [13], sol–gel process [14], and so forth. Amongst all these techniques, the sol–gel is suitable to grow low-cost ZOTFs over wide area that is effective for practical purposes. In addition, it is easy to tune various parameters related to the sol-gel process. Thus, this technique has widely been utilized as an alternative approach to the vacuum based ZOTFs deposition method. In the sol-gel process, various inorganic (nitrates, perchlorates and chlorides) or organic-based (acetates and acetylacetonates) salts are used in alcohol to form the alkoxide or alkoxy-complex subsequent to the oxide development through the hydrolysis/polymerization reaction. Vacuum-based methods can effectively be used to achieve ZOTFs doped with In with optimum film thicknesses where the thermal annealing can further reduce the electrical resistivity up to 1.3×10^{-2} Ω.cm [15]. To diminish the electrical resistivity of the group III elements-doped ZOTFs further using the sol–gel process, some careful preparation and comprehensive characterizations are still needed [16]. Based on these factors, pure and Al-doped ZnO nanofilms (AZONFs) were deposited on the Si substrate via the sol–gel allied spin coating method and characterized using different analytical tools. The structural, morphological, electrical, and optical properties of the deposited AZONFs were determined as a function of different Al concentrations.

2. Experimental procedures

The AZONFs were grown on the p-type Si (100) substrate via the sol–gel allied spin coating approach. Highly pure chemicals (Alfa Aesar, Merck, 99.999%) were selected for the sample preparation. Zn precursor solution was made using zinc acetate dihydrate (ZnAc) [$Zn(CH_3COO)_2.2H_2O$] after dissolving it into 0.1 M 2-propanol (C_3H_8O as solvent) and ethanolamine (EA as stabilizer). To obtain a clear and stable solution, EA was mixed. The molar ratio of ZnAc to EA was fixed at 1:1 and aluminum nitrate nonahydrate [$Al(NO_3)_3\cdot9H_2O$] was added into the mixture for the Al dopants with different contents (0, 1, 2, 3, 4 and 5 at%). The resultant solution was stirred magnetically at 60 °C for 90 min to get a clear and homogenous mixture. After 24 h, the transparent solution was used for the spin coating onto the Si (100) substrates. Later, the coating and drying process was conducted for approximately 30 sec at the speed of 3000 rpm. The deposited AZONFs were dried inside an electrical furnace for 10 min at 300 °C, where the coating to drying was repeatedly (10 times) carried out. Next, the dried AZONFs were subjected to the thermal annealing process at 500 °C (at the rate of 5 °C/ min) for 3 h.

The crystallinity and structural properties of the as-deposited AZOTFs were examined by the X-ray diffraction measurement. The X-ray diffraction measurement was done using Bruker D8 Advance X-ray Diffractometer that used Cu $K\alpha_1$ line of wavelength 1.5406 Å. The XRD patterns were recorded at the scanning angle (2θ) range from 20 to 80°. The scan rate of 1.2° per min at a resolution of 0.01° was used. The surface morphologies of the prepared samples were imaged using the field emission scanning electron microscopy (FESEM, ZEISS SUPRA 35 VP). The elemental traces within the nanofilms were determined using the energy dispersive X-ray (EDX) spectroscopy. The photoluminescence (PL) emission spectra of

the samples were measured using a Perkin Elmer LS 55 Luminescence Spectrometer. The spectrometer operated at excitation wavelength of 320 nm using a Xenon-flash lamp. All the characterizations of the AZONFs were conducted at room temperature.

3. Results and discussions

3.1 Structural analyses

Figure 1 displays the XRD profiles of ZONFs without and with different amounts of Al doping. The intense XRD peaks due to the Bragg diffraction from the ZnO nanocrystalline lattice were matched to the JCPDS card no. 36–1451 [17]. All the AZONFs exhibited the single-phase ZnO hexagonal wurtzite crystal structure with the preferred growth along (100), (002) and (101) lattice directions planes (intense peaks) and minor peaks along (102), (110), (103) and (201) orientations and corresponded to the angular positions of 31.86°, 34.42° and 36.28°, 47.68°, 56.53°, 62.92° and 67.36°. In addition, the XRD pattern did not show any other peaks, indicating the complete absence of any secondary crystal or impurity phases like Al_2O_3, $ZnAl_2O_4$ and glassy ZnO. The studied AZONFs enclosing 1 at% of Al showed the most intense XRD peak at 36.28° which indicated the preferred lattice growth along (101) direction with the c-axis normal to the substrate plane. The XRD peak intensities of the AZONFs were reduced with the increase in the Al doping levels, implying the deteriorations in the crystallinity of the samples. The observed declination in the nanofilms (NFs) crystallinity was ascribed to the Zn and Al ionic size mismatch related induced stress and segregated Al at the grain boundary [18]. The intense peaks of the AZONFs were shifted to higher angles when the Al doping levels were raised, confirming the successful incorporation of Al into the ZnO lattice structures. This shift in the XRD peak position was mainly due to the replacement of Zn by Al in the hexagonal crystal structure [19] and subsequent decrease in the lattice parameters [20].

Table 1 depicts the changes in the full width at half maximum (FWHM) values, nanocrystallite size, cell parameters (*a* and *c* of the hexagonal ZnO structure), and unit cell volume of the prepared AZONFs as a function of Al contents. The nanocrystallite size (D) in the film was evaluated via the Scherrer formula by analyzing the most intense (101) XRD peak [21]:

$$D = \frac{0.9\lambda}{\beta cos\theta} \tag{1}$$

where λ is the X-ray wavelength (1.5406 Å), β is the FWHM) of the XRD peak at location of θ. The nanocrystallite sizes in the films were reduced from 28.31 to 18.63 nm with the rise of Al doping level from 0 to 5 at%.

The values of *a* and *c* were calculated by analyzing the (100) and (002) XRD peaks [22]:

$$a = \frac{\lambda}{\sqrt{3}sin\theta_{100}} \tag{2}$$

$$c = \frac{\lambda}{\sin\theta_{002}} \tag{3}$$

The estimated *c/a* value of the proposed AZONFs matched with the JCPDS Card No. 36-1451 for the ZnO bulk crystal [23]. The crystal density (d) and unit cell volume (V) of the hexagonal lattice structure in the films was obtained using [24]:

$$d = \frac{1.6609.M.n}{V} \quad (4)$$

$$V = 0.866\, a^2 c \quad (5)$$

where M and n are the molecular weight and formula units number in the hexagonal ZnO unit cell (n = 2).

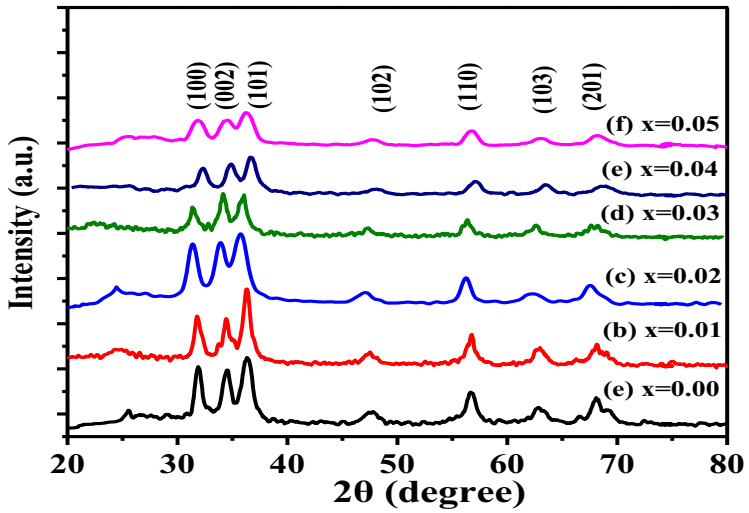

Figure 1. XRD profiles of the studied AZONFs.

The densities of the NFs were decreased (Table 1) with the increase of Al contents, which was ascribed to the lower atomic mass of Al (26.982) compared to ZnO (81.38). The values of *a* and *c* were increased the rising level of Al, leading to a reduction in the unit cell volume as well as crystalline density. In fact, in the crystal lattice sites the Zn^{+2} were replaced by the Al^{+2} and their ionic size mismatch, presence of point defects, extended defects, dislocations as well as the cation and anion vacancies were responsible for reduction in the density of the NFs (Table 1). Emergence of these lattice imperfections in the AZONFs could alter their crystalline density and mechanical properties. At lower doping level of Al, the nanocrystallite sizes were not influenced by such imperfections because of the neutralizations. However, at higher doping level, the nanocrystallite sizes and micro strain in the AZONFs were dependent on the film thickness. Thus, the reduction in the crystalline density with the rising level of Al implied the expansion in the lattice volume, leading to an enhancement in the *c/a* values of the AZONFs. This result is also supported by the XRD data.

Table 1. Al contents dependent changes in the nanocrystallite sizes, FWHM, lattice constants, densities, resistivities and optical band gap energies of the AZONFs obtained from the XRD peak analyses.

Al contents (at.%)	**D (nm)**	**FWHM $\times 10^{-3}$ (Rad)**	***a*** **(Å)**	***c*** **(Å)**	***c/a***	***d*** **(gm/cm^3)**	**ρ (Ω.cm)**	**E_g (eV)**
0	28.31	5.3825	3.24969	5.20663	1.60219	5.67718	29.628	3.218
1	26.86	5.6730	3.24979	5.20722	1.60232	5.63824	04238	3.245
2	25.07	6.0781	3.24989	5.20766	1.60241	5.59948	08.194	3.262
3	22.93	6.6452	3.24999	5.20825	1.60254	5.56056	10.023	3.281
4	20.17	7.5544	3.25009	5.20884	1.60267	5.52168	18.884	3.293
5	18.63	8.1788	3.25019	5.20942	1.60280	5.48281	20.108	3.304

3.2 Morphology analyses

Figure 2 shows the FESEM micrographs (top view) of the prepared AZONFs. The surface of the first three NFs revealed nearly homogeneous morphologies (Figure 2A, 2B and 2C) with well-developed nanocrystallites which is more prominent in the undoped sample. The pure NF (Figure 2A) and the one with 1.0 at.% of Al (Figure 2B) were composed of nanoflakes (NFs), nanosheets (NSs) and nanorods (NRs). The denser nanostructures with less porosity with larger crystallites were observed. The nanorods were broad and distributed inhomogeneously on the substrate surface. The AZONFs containing 1 at.% of Al (Figure 2B) displayed elongated NRs together with some voids. The diameters, heights and densities of these nanorods were considerably altered with the Al contents, which was ascribed to the formation of the nucleation sites. In addition, the NRs growth rate and directions were significantly influenced by the variation of the Al levels [25]. In the present work, the NF containing 2 at.% of Al (Figure 2C) displayed three kinds of nanostructures including the irregular nanoparticles (NPs), some speckled nanosheets and nanoflakes with varying orientations which agrees with other literature report [26]. This NF showed aggregated nanostructures generated from the initial grain and extended to the particles after forming the critical nuclei. The NF containing 3 at.% of Al (Figure 2D) revealed nanoparticles and nanoflakes morphologies which were clustered together with horizontal orientation respecting the substrate. In addition, some small grains were observed which regarded as the attributes of the sol–gel process and was consistent with reported findings [21]. The NF prepared with Al contents of 4 at.% (Figure 2E) and 5 at.% (Figure 2F) disclosed nanoparticles and nanoflakes morphologies which were comparable with the previous works [27,28].

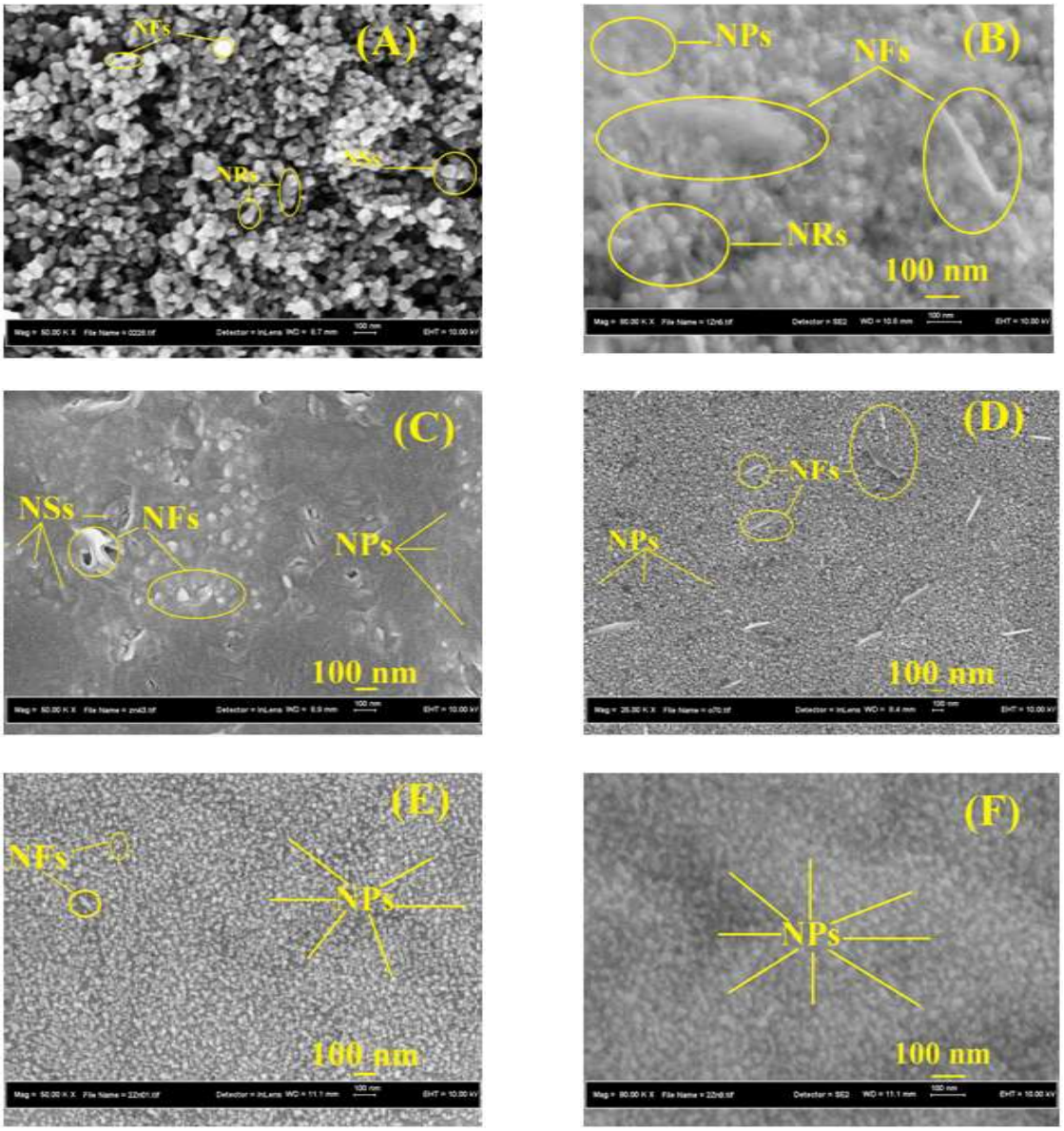

Figure 2. FESEM images of the AZONFs with Al contents of (A) 0, (B)1, (C) 2, (D) 3, (E) 4 and (F) 5 at.%.

Figure 3 illustrates the EDX spectrum of the typical AZONFs with 1 at.% of Al, which detected the presence of the chemical species such as Si, Zn, O and Al atoms without any impurities. The observation of the appropriate elemental traces in the AZONFs could support the XRD results. Upon thermal annealing, the amounts of Zn and O in the NFs were reduced, implying the vaporization of some loosely bound Zn on the surface and diffusion within the Si substrate followed by intermixing. The EDX data for Al obtained

from the upper part of the AZONFs was approximately 1 at.% which is consistent with the doping content of Al in the NFs corresponding to the sol-gel growth solution.

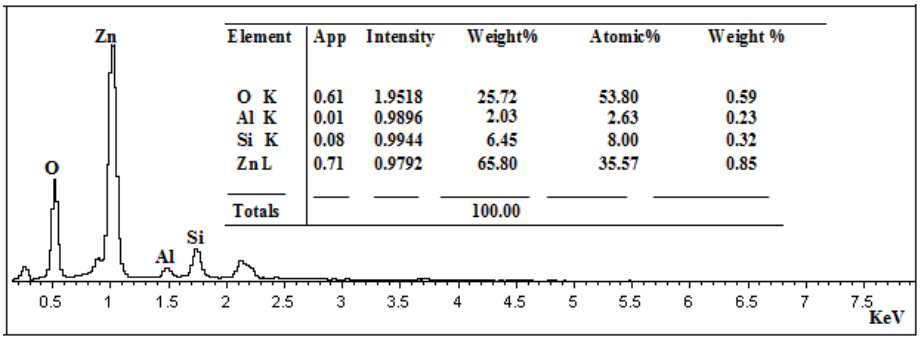

Element	App	Intensity	Weight%	Atomic%	Weight %
O K	0.61	1.9518	25.72	53.80	0.59
Al K	0.01	0.9896	2.03	2.63	0.23
Si K	0.08	0.9944	6.45	8.00	0.32
Zn L	0.71	0.9792	65.80	35.57	0.85
Totals			100.00		

Figure 3. EDX spectrum of the typical AZONFs with 1 at.% of Al.

3.3 Resistivity Measurements

Figure 4 displays the measured electrical resistivity of various films made with different Al contents. The resistivity of the film was radically dropped at 1 at.% of Al (lowest value of 4.238×10^{-3} Ω.cm) and then increased steadily with the increase in Al contents beyond 1 at.% [28]. The electrical resistivity of the NFs was dependent directly on the electrons density generated via the ionization of the interstitial Zn atoms and O vacancies [29]. The observed enhancement in the electrical resistivity with the increase in the Al contents was ascribed to the improved carriers' mobility aroused from the segregated Al dopants at the grain boundaries. In fact, the dopant Al ions participated as electrical carriers at lower contents. However at higher doping level, the separation of Al at the grain boundaries of the lattice led to the lowering in the resistivity. The resistivity of the Al-doped NFs were inversely proportional to the dominance of the (002) and (101) growth planer orientations [30]. The increase in the resistivity of the film beyond 1 at.% of Al was due to the decrease in the carriers' density when Al contents were excess, leading to the decrease in the carriers' mobility. It was argued that excessive amounts of Al in the NFs can form non-conducting clusters of Al_2O_3, resulting in the crystalline disorder and defects generation which in turn trap the carries rather than acting as electron donors [31]. It is asserted that the decrease in the nanocrystallite size with the increase in the Al doping contents indeed lowered the carriers' mobilities and enhanced the electrical resistivity of the NFs which is consistent with the other report [32].

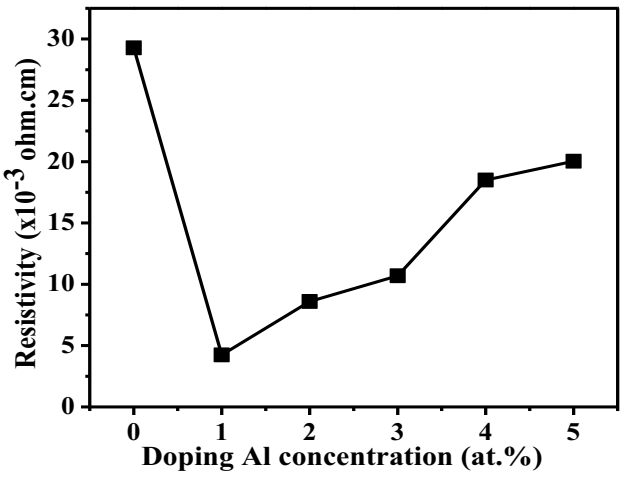

Figure 4. Al contents dependent electrical resistivity of the AZONFs.

3.4 PL spectra

Figure 5 displays the Al contents dependent room temperature PL emission spectra of the AZONFs obtained at the excitation wavelength of 320 nm. The emission spectra revealed two prominent peaks due to the characteristic near-band edge (NBE) emission in wurtzite structure ZnO (intense purple emission at around 380 nm) emerged from the excitons annihilation [33-35] and due to the interstitial oxygen ions (broad orange emission at 600 nm) [36]. The intensities of both PL peaks shown by the AZONFs were decreased with the increase in the Al contents. The NBE emission peaks of the film showed a blue shift and the minor peak revealed a small red shift. In the doped film, more free carriers from the Al dopants occupied the energy states positioned at the conduction band (CB) bottom. Upon their excitations, the excitons occupied the higher energy states at the CB bottom. As the Al contents were increased, the band-to-band transitions dominated the NBE emission and the radiative recombination of the excitons led to the blue shift of the intense PL peak [37, 38]. The observed reduction in the intensities of the intense peak of the NFs with the increase in the Al contents was due to the enhancement of the nonradiative defects [39-42]. According to Srikant and Clarke [41], the UV peak at around 395 nm is to the shallow donors that may arise from complex defects of the Zn interstitials as argued [43].

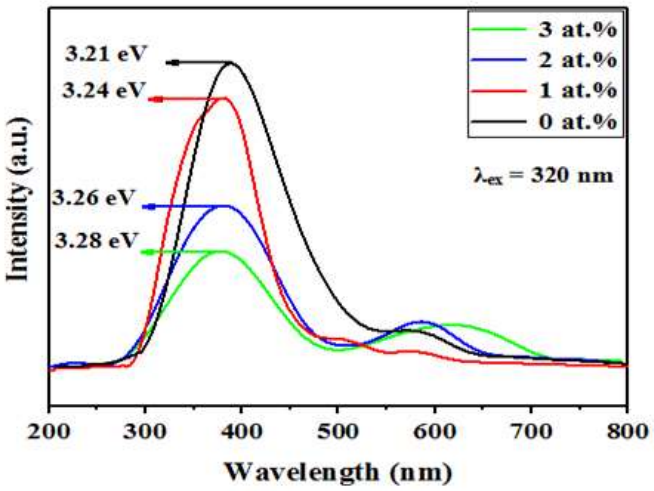

Figure 5. Al contents dependent PL spectra of the AZONFs.

4.Conclusions

Al-doped ZONFs with diverse morphologies and nanocrystalline structure were prepared on Si substrates via the sol–gel unified spin-coating strategy and characterized. The dependence of the room temperature structure, morphology, photoluminescence and resistivity of the AZONFs on the varying Al doping levels were discerned. The XRD analyses confirmed the good polycrystalline nature of the deposited NFs with hexagonal wurtzite structure. The crystallinity, PL peak intensity and electrical resistivity of NFs were decreased with the increase in the Al contents which were attributed to the segregation of Al, replacement of the Zn sites in the lattice, and their ionic radii mismatch. The nanocrystallite size in the films was ranged from 28 to 18 nm. The obtained NFs revealed homogeneous and continuous surface morphologies. The conductivity of the NFs was improved due to Al doping where the lowest resistivity achieved at 1 at.% of Al (4.238×10^{-3} Ω.cm). The optical band gap energy of the NFs was increased with the increase in the Al contents. The proposed AZONFs may be useful for sundry optoelectronic and photovoltaic applications.

Acknowledgments

The authors are grateful to the Higher Education and Scientific Research, University of Al-Qadisiyah, Faculty of Education, Physics Department of Iraq for financial support.

References

[1] Ismail, B., M. Abaab and B. Rezig 2001 *Thin Solid Films* **383** 1 pp. 92-94
[2] Wang, D., J. Zhou and G. Liu 2009 *Journal of Alloys and Compounds* **481** 1 pp. 802-805
[3] Xue, S., X. Zu, W. Zhou, H. Deng, X. Xiang, L. Zhang and H. Deng 2008 *Journal of Alloys and Compounds* **448** 1 pp. 21-26
[4] Shinde, V., C. Lokhande, R. Mane and S.-H. Han 2005 *Applied Surface Science* **245** 1 p. 407-413
[5] Sanchez-Juarez, A., A. Tiburcio-Silver and A. Ortiz 1998 *Solar energy materials and solar cells* **52** 3 p. 301-311

[6] Jin, Z.C., I. Hamberg and C. Granqvist 1988 *Journal of applied physics* **64** 10 p. 5117-5131
[7] Zhou, H.-m., D.-q. Yi, Z.-m. Yu, L.-r. Xiao and J. Li 2007 *Thin solid films* **515** 17 p. 6909-6914
[8] Kuo, S.-Y., W.-C. Chen, F.-I. Lai, C.-P. Cheng, H.-C. Kuo, S.-C. Wang and W.-F. Hsieh 2006 *Journal of crystal growth* **287** 1 p. 78-84
[9] Joseph, M., Tabata, H. and Kawai, T 1999 *Applied physics letters* **74** 17 pp.2534-2536
[10] Kashiwaba, Y., Katahira, F., Haga, K., Sekiguchi, T. and Watanabe, H 2000 *Journal of Crystal Growth* **221** 1 pp.431-434
[11] Minami, T., Nanto, H. and Takata, S 1984 *Japanese Journal of Applied Physics* **23** 5A p.L280
[12] Cembrero, J., A. Elmanouni, B. Hartiti, M. Mollar and B. Marı 2004 *Thin Solid Films* **451** p. 198-202
[13] Andrade, E. and M. Miki-Yoshida 1999 *Thin Solid Films* **350** 1 p. 192-202
[14] Al-Asedy, H.J. and Al-khafaji, S.A 2020 *Applied Physics A* **126** 9 pp.1-10
[15] Wang, F.-H., H.-P. Chang, C.-C. Tseng, C.-C. Huang and H.-W. Liu 2011 *Current Applied Physics* **11** 1 p. S12-S16
[16] Çopuroğlu, M., S. O'Brien and G.M. Crean 2009 *Thin Solid Films* **517** 23 p. 6323-6326
[17] Park, M., & Han, S. M. 2015 *Thin Solid Films* **590** p.307-310
[18] Zhou, H. M., Yi, D. Q., Yu, Z. M., Xiao, L. R., & Li, J 2007 *Thin solid films* **515** 17 p.6909-6914
[19] Kim, H., Pique, A., Horwitz, J. S., Murata, H., Kafafi, Z. H., Gilmore, C. M., & Chrisey, D. B 2000 *Thin solid films* **377** p. 798-802
[20] Shahzad, M. B., Qi, Y., Lu, H., & Wang, X 2013 *Thin solid films* **534** pp.242-248
[21] Al-Asedy, H.J., Bidin, N., Abbas, K.N. and Al-Azawi, M.A 2018 *Materials Research Bulletin* **97** pp.71-80
[22] Al-Asedy, H.J., Bidin, N., Abbs, K.N. and Al-Azawi, M.A 2016 *Modern Applied Science* **10** 4 pp.12-20
[23] Al-Asedy, H.J., Ati, A.A., Bidin, N. and Lee, S.L 2017 *Applied Physics A* **123** 10 p.665
[24] Al-Asedy, H.J., Al-Khafaji, S.A., Bakhtiar, H. and Bidin, N 2018 *Applied Physics A* **124** 3 p.223
[25] Henni, A., Merrouche, A., Telli, L., & Karar, A 2016 *Journal of Electroanalytical Chemistry* **763** pp.149-154
[26] Bu, I. Y 2011 *Journal of Alloys and Compounds* **509** 6 pp.2874-2878
[27] Çopuroğlu, M., O'Brien, S., & Crean, G. M 2009 *Thin Solid Films* **517** 23 pp.6323-6326
[28] Zhou, H. M., Yi, D. Q., Yu, Z. M., Xiao, L. R., & Li, J 2007 *Thin solid films* **515** 17 pp. 6909-6914
[29] Sukkar, M. H., & Tuller, H. L 1982 *Advances in Ceramics* **7** p. 71
[30] Lee, J. H., & Park, B. O 2003 *Thin Solid Films* **426** 1pp. 94-99
[31] Hu, J., & Gordon, R. G 1992 *Journal of Applied Physics* **71** 2 pp. 880-890
[32] El Manouni, A., Manjón, F. J., Mollar, M., Marí, B., Gómez, R., López, M. C., and Ramos-Barrado, J. R 2006 *Superlattices and Microstructures* 39 1 pp.185-192
[33] Yan, C., & Xue, D2008 *Journal of Crystal Growth* **310** 7 pp. 1836-1840
[34] Salim, A. A., Ghoshal, S. K., Krishnan, G., and Bakhtiar, H 2020 *Materials Letters* **264** p. 127335
[35] Islam, S., Bakhtiar, H., Bidin, N., Salim, A. A., Riaz, S., Abbas, K. N and Naseem, S. 2018 *Journal of Saudi Chemical Society* **22** 7 pp.826-83
[36] Greene, L. E., Law, M., Goldberger, J., Kim, F., Johnson, J. C., Zhang, Y., and Yang, P 2003 *Angewandte Chemie International Edition* 42 26 pp. 3031-3034
[37] Chen, Y. W., Liu, Y. C., Lu, S. X., Xu, C. S., Shao, C. L., Wang, C., ... & Fan, X. W. 2005 *The Journal of chemical physics* **123** 13 pp. 134701

[38] Salim, A. A.., & Bidin, H. B 2018 *Journal of Advanced Research in Materials Science* **43** 1 pp.28-33
[39] Jeong, S. H., Kim, J. K., & Lee, B. T 2003 *Journal of Physics D: Applied Physics* **36** 16, pp.17-20
[40] Salim, A. A., Ghoshal, S. K., Suan, L. P., Bidin, N., Hamzah, K., Duralim, M., & Bakhtiar, H 2018 *Malaysian Journal of Fundamental and Applied Sciences* **14** 3-1 pp. 447-449
[41] Srikant, V., & Clarke, D. R 1998 *Journal of Applied Physics* **83** 10 pp. 5447-5451
[42] Salim, A. A., Bidin, N., & Ghoshal, S. K 2018 *LWT* **90** pp.346-353
[43] Look, D. C., Hemsky, J. W., & Sizelove, J. R 1999*Physical review letters* **82** 12 p.2552